RASĀYAN *J. Chem.*
Vol. 19 | No. 1 | 492-497 | January-March | 2026
ISSN: 0974-1496 | e-ISSN: 0976-0083 | CODEN: RJCABP
http://www.rasayanjournal.com
http://www.rasayanjournal.co.in

ROLE OF DEFECTS AND CRYSTALLITE SIZE OPTIMIZATION IN ENHANCING THE CATALYTIC ACTIVITY OF Zn-DOPED MoO_3

Vaishali B. Raut[1], Supriya S. Shukla[2], and Sharda R. Gadale[1,✉]
[1]Department of Chemistry, Yashwantrao Mohite College of Arts, Science and Commerce, Pune, Bharati Vidyapeeth (Deemed To Be University), Pune-411038, (Maharashtra) India
[2]Department of Physics, Yashwantrao Mohite College of Arts, Science and Commerce, Pune, Bharati Vidyapeeth (Deemed To Be University), Pune-411038, (Maharashtra) India
✉Corresponding author: dagade@rediffmail.com

ABSTRACT

Zn-doped MoO_3 nano-particles were synthesised by citric acid-assisted sol-gel method with doping concentrations of 2%, 4%, 6%, 8%, and 10%, with an objective to enhance their structural and biological functionalities. The orthorhombic α-MoO_3 phase in all samples, with a size ranging from 45.2 nm (pure MoO_3) to 27.6 nm at 10% Zn doping, shows significant lattice strain and defect formation during X-ray diffraction (XRD) analysis. FTIR spectra exhibited characteristic Mo-O stretching vibrations at 993 and 870 cm^{-1}, with minor red shifts upon doping. Antibacterial activity increased with both doping level and concentration. The 10% Zn-MoO_3 at 10 mg mL^{-1} displayed the highest zones of inhibition-25 mm (*Bacillus*), 20 mm (*Pseudomonas*), 19 mm (*S. aureus*), and 16 mm (*E. coli*). Antioxidant assays revealed dose-dependent radical scavenging, with 10% Zn-MoO_3 achieving 26.97% inhibition at 1000 µg mL^{-1}, while ascorbic acid reached 97.56% under the same conditions. These findings confirm that Zn doping significantly modifies the structural framework of MoO_3, creating surface defects and oxygen vacancies that contribute to enhanced antimicrobial and antioxidant activity, positioning these nanomaterials as promising agents for biomedical and catalytic applications.

Keywords: Zn-doped MoO_3, Nanomaterials, Size Optimisation, Photocatalytic, Antimicrobial, Antioxidant Activity.

RASĀYAN *J. Chem.*, Vol. 19, No.1, 2026

INTRODUCTION

Molybdenum trioxide (MoO_3) and exceptional physicochemical properties of transition metal oxides make it a suitable candidate for research and development. The orthorhombic α-MoO_3 phase, due to its high surface area, layered structure, and exceptional redox behavior make it thermodynamically stable and is frequently employed in photocatalysis and antimicrobial systems.[1,2] Recent studies on zinc-integrated molybdenum-based nanomaterials, including ZnO/MoO_3 heterostructures, Zn-doped MoS_2 nanosheets, and Zn–MoOx mixed oxides, have demonstrated that zinc incorporation significantly enhances photocatalytic charge separation, fosters oxygen vacancy creation, and elevates redox activity. These compelling findings support our pursuit of Zn-doped MoO_3 nanoparticles to harness similar defect engineering and catalytic performance enhancements. Despite these advantages, the pristine form of MoO_3 often suffers from inherent limitations due to its dialectical weakness and surface reactivity, which restrict its functional performance in advanced applications. The effective way to overcome these inadequacies is metal ion doping, which alters the crystal lattice, introduces oxygen vacancies, and modifies electronic structures. The changes enhance the material's catalytic, electrical, and biological activity by improving charge separation, increasing surface defects, and producing active sites.[3,4] Zinc (Zn), a divalent transition metal with a comparable ionic radius to molybdenum, has been identified as a promising dopant. Incorporating Zn into the MoO_3 lattice creates lattice distortions and oxygen vacancies, enhancing redox characteristics and improving antibacterial and photocatalytic capabilities.[5,6] In several studies, Zn-doped MoO_3 nanoparticles exhibit excellent antibacterial and antifungal properties associated with their undoped counterparts, primarily due to improved reactive oxygen species (ROS) and disruption of microbial membranes.[7,8] The biological activity, Zn-doped MoO_3, shows enhanced photocatalytic

http://doi.org/10.31788/RJC.2026.1919432

efficiency in the disintegration of organic pollutants, attributed to improved charge transport and defect engineering. These findings position Zn-doped MoO_3 as a multifunctional nanomaterial capable of addressing the challenges in the field of environmental and biomedical. The synthesis technique is helpful in determination of Dopant dispersion in nanomaterials, size, and morphology. Among various techniques, the sol-gel technique provides remarkable advantages like low processing temperatures, homogeneous dopant distribution, and fine regulation over the final particle size. This technique allows the formation of structurally uniform and chemically stable metal oxide nanostructures with high purity, which are essential for reproducible functional performance. By systematically varying Zn concentrations and employing advanced analytical techniques, we seek to understand the correlation between defect engineering and biological functionality.

EXPERIMENTAL

Material and Methods

All chemicals utilised in this investigation were analytical grade. Ammonium heptamolybdate tetrahydrate [$(NH_4)_6Mo_7O_{24}\cdot 4H_2O$; CAS No. 12054-85-2] and zinc nitrate hexahydrate [$Zn(NO_3)_2\cdot 6H_2O$; CAS No. 10196-18-6] were purchased from SRL (Srichem, India), ensuring high purity for reproducible synthesis. Deionised water was used in the synthesis and washing processes. Mueller–Hinton agar (M173) and 2,2-diphenyl-1-picrylhydrazyl (DPPH; RM2798) were used for antimicrobial and antioxidant assays, respectively. Microbial experiments were conducted using ATCC standard strains under sterile conditions.

Synthesis of Zn-Doped MoO_3

Zn-doped MoO_3 nanoparticles were synthesised using sol-gel and co-precipitation techniques. Initially, 24.54 g of ammonium heptamolybdate tetrahydrate [$(NH_4)_6Mo_7O_{24}\cdot 4H_2O$] was dissolved in 30 mL of deionised water and stirred until a clear solution was obtained. For dopant incorporation, zinc acetate was added at varying concentrations (2%, 4%, 6%, 8%, and 10% w/w), as outlined in the Table-1. The pH was carefully adjusted to ~9 using 3% aqueous ammonia to promote precursor complex formation and sol stabilisation. A few drops of dilute nitric acid (HNO_3) were added, and then the solution was heated in a sand bath to get a stable polymeric network. After cooling, the resultant gel was washed to remove residual ions and acid. The product was subsequently centrifuged, vacuum dried, and calcined at 500 °C for 3 hours in a muffle furnace. The final heating treatment removed organic residues, enhanced crystallinity, and effectively incorporated Zn^{2+} into the MoO_3 lattice.

Table-1: Composition and Sample Preparation for Zn-Doped MoO_3

Zn Doping (%)	Zinc Acetate (g)	DI Water (mL)	AHM (g)	NH_3 (3%) (mL)
2%	5.394	10-12	24.54	1-2
4%	10.788	15-18		
6%	16.17	20-25		
8%	21.56	30		
10%	26.96	30		

Characterization

X-ray diffraction (XRD) analysis was performed at our institute, using a Bruker Phaser-D2 diffractometer with Cu-Kα radiation (λ = 1.5406 Å) operated at 40 kV and 30 mA. The crystalline structure and phase purity were confirmed across a 2θ range of 10°-70°. Analysis by using an Agilent Technologies Spectrum- FTIR Two spectrometer- over 4000–400 cm^{-1}, revealing characteristic Mo=O (814–877 cm^{-1}), Zn–O (423–531 cm^{-1}), and O–H (~3300 cm^{-1}) vibrational modes, confirming successful Zn incorporation was carried out. Surface morphology and particle size were analysed by using FESEM, ZEISS EVO-18. The elemental composition and dopant distribution were confirmed through Energy-Dispersive X-ray Spectroscopy (Oxford Instruments) integrated with FESEM. Raman spectroscopy conducted using a LabSpec 6 from Horiba Scientific, a spectrometer with a 532 nm laser source, provided insight into vibrational modes associated with Mo–O bonds, highlighting structural distortions and defect formations due to Zn doping.

Antimicrobial and Antioxidant Activity

Zn-doped MoO_3 nanoparticles were tested for antibacterial activity against clinically important pathogens, including *Staphylococcus aureus*, *Bacillus subtilis*, *Escherichia coli*, *Pseudomonas aeruginosa*, and *Candida albicans*, using the agar well diffusion method. Nanoparticle suspensions at concentrations of 25, 50, and 100 µg/mL were introduced into 6 mm wells on Mueller–Hinton agar plates inoculated with the test organisms. After a 24-hour incubation at 37°C, the Zn-doped MoO_3 nanoparticles demonstrated concentration-dependent antibacterial activity, as determined by zones of inhibition. The antioxidant activity of Zn-doped MoO_3 nanoparticles was assessed using the DPPH test. DPPH (1,1-diphenyl-2-picrylhydrazyl) is a persistent free radical that has a deep violet colour and turns yellow when reduced by an antioxidant. In a microtiter plate, combine 100 µL of nanoparticle solution with 100 µL of 0.1% methanolic DPPH and incubate for 30 minutes in the dark. The extent of discolorations, indicating radical scavenging, was observed visually and quantified at 490 nm using an ELISA plate reader.

RESULTS AND DISCUSSION

The XRD pattern of Zn-doped MoO_3 nanoparticles confirms their crystalline nature, with all peaks indexed to the orthorhombic α-MoO_3 phase (JCPDS card No. 05-0508), was performed. No additional peaks corresponding to ZnO or MoO_2 phases were detected, indicating the MoO_3 structure remains intact despite Zn incorporation. At 2% doping, intense, and sharp peaks (notably at 2θ ~12.8°, 23.3°, 25.7°, and 27.4°) confirm high crystallinity. As Zn content increases (4–10%), peak broadening and intensity reduction are observed, indicating increased lattice strain and decreased crystallite size. This effect is due to the substitution of Mo^{6+} ions (ionic radius: 0.59 Å) by smaller Zn^{2+} ions (ionic radius: 0.60 Å), creating structural defects and oxygen vacancies. At 10% doping, peak degradation suggests partial amorphisation or secondary phase emergence. The average crystallite size, computed using the Scherrer formula, falls as Zn content increases, indicating the presence of internal lattice stress and defect development.

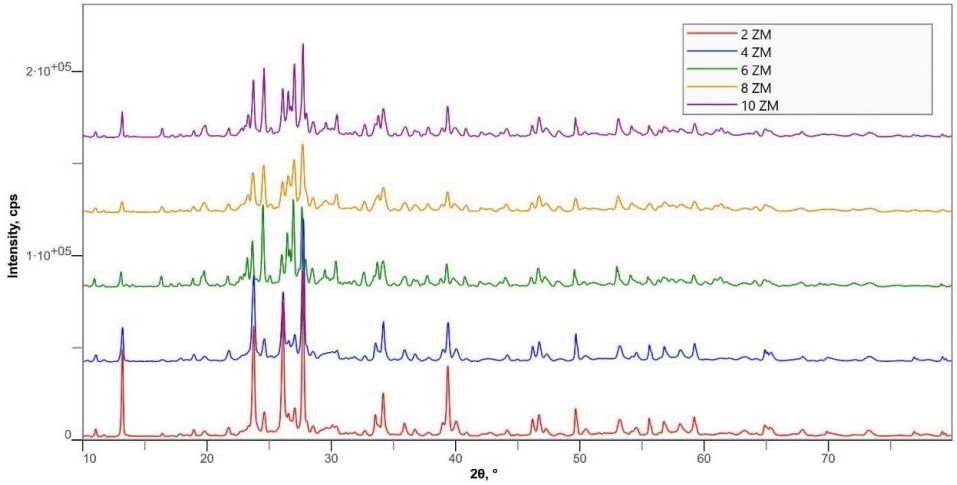

Fig.-1: XRD Patterns of Zn-Doped MoO_3 Nanoparticles at different Levels of Concentration

The FTIR spectra (Agilent Technologies) of Zn-doped MoO_3 nanoparticles reveal structural changes due to Zn incorporation. Characteristic Mo=O stretching vibrations were found around 814-878 cm^{-1}, confirming the MoO_3 structure. The emergence of Zn–O bond vibrations near 423–493 cm^{-1} indicates successful Zn doping. Broad absorption bands around 3330 cm^{-1} and peaks near 1618 cm^{-1} correspond to O–H stretching and H–O–H bending vibrations, respectively, suggesting the presence of adsorbed water or hydroxyl groups.

FESEM-EDS

The FESEM (Zeiss) images of Zn-doped MoO_3 nanoparticles (2–10% doping) exhibit clear morphological evolution with increasing Zn content. At 2% doping, particles are densely packed and uniformly distributed with minimal agglomeration, indicating good dopant dispersion. EDS confirms the presence of Mo, O, and Zn, with Zn content aligning with the intended doping level (~4.73 at %).

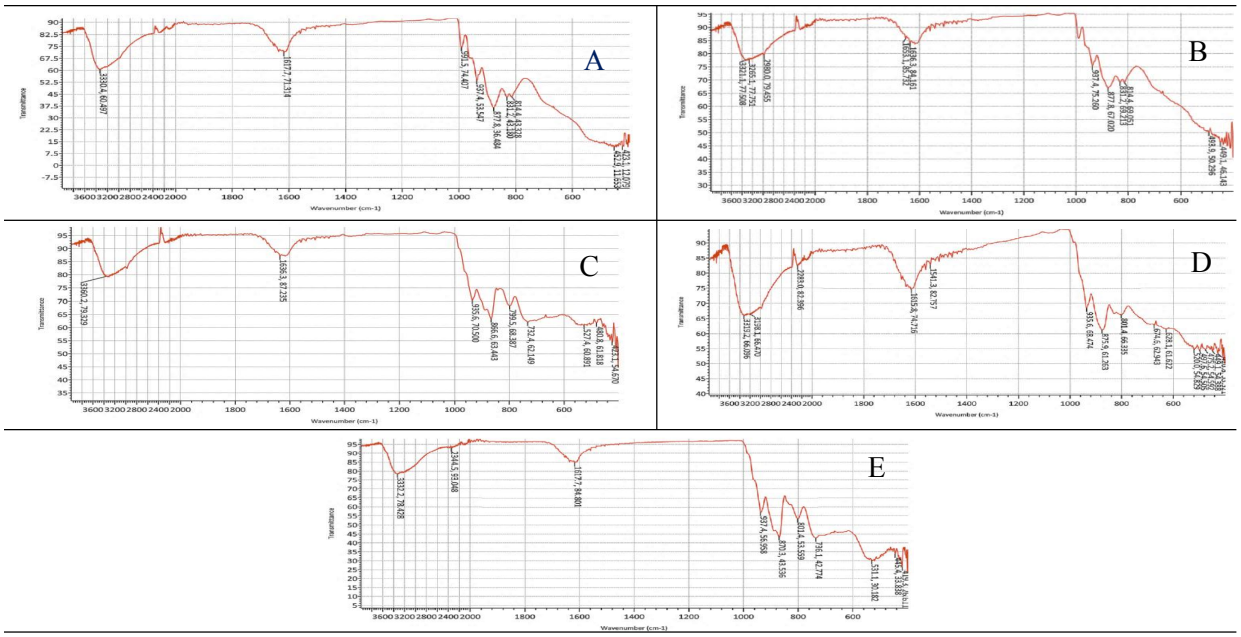

Fig.-2: FTIR Patterns of Zn-Doped MoO_3 Nanoparticles at different Concentration Levels (A) 2%, (B) 4%, (C) 6%, (D) 8%, and (E) 10% respectively

With 4% doping, particles appear more defined and slightly larger, showing improved crystallinity and reduced clustering. At 6%, FESEM reveals a rougher, porous texture and irregular shapes, suggesting lattice strain and enhanced surface area. EDS mapping continues to show homogeneous Zn distribution. At 8% doping, finer particles with a smoother surface emerge, likely due to coalescence or sintering effects. The Zn content increases proportionally, with no visible phase separation. However, at 10% Zn, the morphology changes drastically, grain boundaries become indistinct, and a dense, film-like structure appears, indicating significant lattice distortion.

Raman Spectroscopy

At 4% Zn, the Mo=O peak remains prominent with minor shifts, and a new low-frequency band emerges at ~133 cm^{-1}, suggesting initial lattice perturbations due to Zn incorporation. Increasing Zn to 6% leads to broadening and weakening of the Mo=O peak (~820 cm^{-1}), along with the appearance of broad bands at higher wavenumbers (~1778–3014 cm^{-1}), indicative of defect states and loss of long-range order, likely due to excess Zn causing structural disorder and oxygen vacancies. At 8% doping, the Mo=O peak becomes less sharp, with additional bands at ~930 and ~967 cm^{-1} suggesting distorted Mo–O bonding, possibly from mixed oxidation states like Mo^{4+}. High-frequency bands (~1464–3007 cm^{-1}) point to defect-induced modes and structural disorder, while a low-frequency peak at ~69 cm^{-1} reflects lattice vibrations affected by heavy doping. At 10% Zn, further disruption is observed with the Mo=O stretching peak at ~823 cm^{-1}, accompanied by peaks at ~971 and ~930 cm^{-1}, signaling extensive Mo–O environment alterations. Additional peaks at ~169~293 and ~664 cm^{-1} suggest reduced order, and a high-wavenumber band at ~2412 cm^{-1} aligns with defect-related scattering.

Antimicrobial and Antioxidant Activity

Table-2 shows antimicrobial observations, the 10% Zn-MoO_3 at 10 mg/mL exhibited the strongest antibacterial activity, with inhibition zones reaching 25 mm for *Bacillus*, 20 mm for *Pseudomonas aeruginosa*, 19 mm for *Staphylococcus aureus*, and 16 mm for *Escherichia coli*. *Bacillus species* were the most sensitive across all doping levels, especially at higher concentrations. In contrast, lower Zn doping levels (2–4%) showed minimal antibacterial activity, indicating that limited Zn incorporation is insufficient to exert strong bactericidal effects. A consistent trend in antimicrobial performance was observed: 10% > 8% > 6% > 4% > 2%. Antifungal experiments on *Candida albicans* indicated similar results, with 10% Zn-MoO_3 providing the strongest suppression (19 mm at 10 mg/mL), though still less effective than the conventional fluconazole (30 mm). The antioxidant potential of Zn-doped MoO_3

nanoparticles (2–10% doping) was assessed via DPPH assay. Ascorbic acid had significant dose-dependent radical scavenging activity, with inhibition increasing from 66.67% at 200 µg/mL to 97.56% at 1000 µg/mL. Whereas $ZnMoO_3$ samples displayed modest antioxidant activity. Among them, 10% $ZnMoO_3$ showed the highest activity, reaching 26.97% inhibition at 1000 µg/mL.

Table-2: Antimicrobial Activity of Zn-Doped MoO_3 Nanoparticles through Zone of Inhibition

Sample	Conc. (mg/ml)	ZOI of				
		E. coli	*S. aureus*	*Bacillus*	*Pseudomonas*	*C. albicans*
Control	-	-	-	-	-	-
Streptomycin	-	29	27	30	32	30
2 %	5	1	1	5	5	2
	10	2	2	10	10	4
4 %	5	4	2	7	7	2
	10	8	5	12	12	6
6 %	5	3	3	9	9	7
	10	6	6	18	18	12
8 %	5	1	2	12	12	4
	10	4	12	20	20	14
10 %	5	12	1	20	20	15
	10	16	19	25	25	19

CONCLUSION

This study shows that zinc (Zn) doping considerably affects the structural and antibacterial characteristics of molybdenum trioxide (MoO_3) nanoparticles. Zn-doped MoO_3 nanoparticles were synthesised using a sol-gel technique, with concentrations ranging from 2% to 10%. Raman spectroscopy revealed that low Zn doping levels (2% and 4%) preserved the orthorhombic α-MoO_3 structure, while higher doping concentrations (6% and above) caused structural distortions, including peak broadening and new vibrational modes, indicating increased defect states and potential amorphisation. Antimicrobial testing against *Escherichia coli, Staphylococcus aureus, Bacillus species, Pseudomonas*, and *Candida albicans* revealed that increasing Zn doping improved activity. Notably, 10% Zn-doped MoO_3 nanoparticles showed the highest zones of inhibition across all examined bacteria, with *Bacillus species* showing the most sensitivity. Higher Zn doping levels are thought to boost antibacterial effectiveness by increasing the formation of reactive oxygen species and structural flaws that jeopardise microbial cell integrity. Zn-doped MoO_3 nanoparticles show promise as antibacterial agents in biomedical and environmental applications align with SDG-9.

ACKNOWLEDGMENTS

I am thankful to my Head of Department of Chemistry Dr. A. B. Pawar, and the Principal, YM College, Pune for providing resources at the different stages of experimentation.

CONFLICT OF INTERESTS

The authors declare that there is no conflict of interest. The co-author has seen and agrees with the contents of the manuscript, and there is no financial interest to report.

AUTHOR CONTRIBUTIONS

The present work is related to *SDG-9: Industry, Innovation, and Infrastructure*. All the authors contributed significantly to this manuscript, participated in reviewing/editing, and approved the final draft for publication. The research profile of the authors can be verified from their ORCID ids, given below:

V. B. Raut https://orcid.org/0009-0008-3586-9546
S.S. Shukla https://orcid.org/0000-0002-1581-8599
S.R. Gadale https://orcid.org/0000-0002-2872-505X

Cite this article as: V. B. Raut *et al.*, *Rasayan J. Chem.*, 19(1), 492-497(2026), https://doi.org/10.31788/RJC.2026.1919432.

REFERENCES

1. M.I. Hidayat, A. Hardiansyah, K. Khoiriah, E. Yulianti, R.A.K. Wardhani, F. Fahrialdi, and M.R.I. Yusuf, *Food Chemistry*, **477**, 143480(2025), https://doi.org/10.1016/j.foodchem.2025.143480
2. N. Jain, R. Paroha, R.K. Singh, S.K. Mishra, S.K. Chaurasiya, R.A. Singh, and J. Singh, *Scientific Reports*, **9**, 2472(2019), https://doi.org/10.1038/s41598-019-38787-1
3. R. Maciejewski, E. Radzikowska-Büchner, W. Flieger, K. Kulczycka, J. Baj, A. Forma, and J. Flieger, *International Journal of Environmental Research and Public Health*, **19**, 11066(2022), https://doi.org/10.3390/ijerph191711066
4. M. Mehmandoust, F. Karimi, and N. Erk, *Chemosphere*, **300**, 134430(2022), https://doi.org/10.1016/j.chemosphere.2022.134430
5. I. Navas, R. Vinodkumar, K.J. Lethy, M. Satyanarayana, V. Ganesan, and V.P. Pillai, *Journal of Nanoscience and Nanotechnology*, **9**, 5254(2009), https://doi.org/10.1166/jnn.2009.1163
6. S. Pang, X. Chang, L. Xu, and J. Wu, *Methods and Applications in Fluorescence*, **13** 025002(2025), https://doi.org/10.1088/2050-6120/ada99b
7. R. Rajakumaran, M. Abinaya, S.M. Chen, K. Balamurugan, and V. Muthuraj, *Ultrasonics Sonochemistry*, **61**, 104823(2020), https://doi.org/10.1016/j.ultsonch.2019.104823
8. M.R. Sokolov, K.A. Tumbinskiy, E.A. Varlamova, A.A. Averin, A.V. Shkolin, and M.A. Kalinina, *ACS Applied Materials & Interfaces*, **15**, 49299(2023), https://doi.org/10.1021/acsami.3c11698

[RJC-9432/2025]